Research Article

Geochemistry of Cenozoic volcanic rocks in Tengchong, SW China: relationship with the uplift of the Tibetan Plateau

Yutao Zhang,[1,*] Jiaqi Liu,[1] and Fanchao Meng[2]

[1]*Key Laboratory of Cenozoic Geology and Environment, Institute of Geology and Geophysics, Chinese Academy of Sciences, Beijing 100029, China (email: iherzolite@sohu.com), and* [2]*College of Geo-resources and Information, China University of Petroleum, Qingdao 266555, China*

Abstract There are wide spread Cenozoic volcanic rocks in Tengchong (CVRT), Yunnan province, SW China. These rocks comprise three rock types: basalt, andesite (dominant type) and dacite. Most samples are sub-alkaline, and among the sub-alkaline rocks, most are high-K calc-alkaline. These rocks have a SiO_2 range of 49.1 wt.% to 66.9 wt.%. TiO_2 contents are not high and have a variation of 0.7 wt.%–1.6 wt.%. Trace element concentrations and element ratios (such as Nb/U, Ce/Pb, Nb/La, etc.) of these rocks have a large variation. $^{87}Sr/^{86}Sr$ values fall in the range of 0.7057–0.7093 and $^{143}Nd/^{144}Nd$ values change from 0.5120 to 0.5125. $^{206}Pb/^{204}Pb$, $^{207}Pb/^{204}Pb$, and $^{208}Pb/^{204}Pb$ ratios are in the range of 17.936–19.039, 15.614–15.810, and 38.894–39.735, respectively. These geochemical characteristics of CVRT make them resemble island-arc volcanic rocks. We suggest that the magmas were generated in the lithospheric mantle that had already been metasomatized by previous subduction processes. By the study of the uplift history of the Tibetan Plateau, we found that the beginning of the geotectonic processes to the eruption of CVRT was coeval with one uplift event. Therefore, we propose that the uplift of the Tibetan Plateau caused collapse of the collisional orogeny in Tengchong, which further triggered the generation and eruption of the CVRT magmas.

Key words: Cenozoic volcanic rocks, geochemistry, petrogenesis, Tengchong, Tibetan Plateau.

INTRODUCTION

Located in the west of Yunnan province, SW China, Tengchong is famous for its geothermal activity, hot springs, and Cenozoic volcanic activity. Cenozoic volcanic rocks occupy vast areas in Tengchong and it is worth noting that most of these volcanic rocks are associated with faults. According to previous researches, there may be magma chambers deep in the crust of Tengchong (Qin *et al*. 2000; Jiang *et al*. 2004; Zhao *et al*. 2006). In consideration that some of these volcanoes have Holocene eruption records, some dormant volcanoes may erupt in the near future, which can be hazardous to both environment and people. The eruption of Cenozoic volcanic rocks in Tengchong (CVRT) seems to have been coupled with the uplift of the Tibetan Plateau and a relationship may exist between them as a result of the particular geotectonic position of Tengchong.

During recent decades, many geological, geophysical, geochemical, and geodetic investigations have been carried out on these volcanic rocks (Mu *et al*. 1987; Tong & Zhang 1989; Bai *et al*. 1994; Kan & Zhao 1994; Han *et al*. 1996; Chen *et al*. 2002; Wang & Huangfu 2004; Wang *et al*. 2007). However, there appears to be no consensus regarding the origin of these volcanic rocks. Zhu *et al*. (1983) and Mu *et al*. (1987) argued that the Tengchong volcanism was derived from the subduction-collision zone between the Indian and Eurasian plates. Zhao and Chen (1992) believed that it was a post-collision arc-volcanism or a

*Correspondence.

Received 25 November 2011; accepted for publication 29 June 2012.

doi:10.1111/j.1440-1738.2012.00819.x

delayed arc-volcanism in the southeast margin of the Tibetan Plateau. Cong *et al.* (1994) proposed that the CVRT were derived from a mature island-arc area. Ji (1998) pointed out that during 5–8 Ma, the lower lithosphere delaminated in Tengchong, resulting in the generation of magmas due to upwelling of the upper mantle. Chen *et al.* (2002) proposed that the magma source for these volcanic rocks was enriched-mantle. This chaos was caused partly by the complex tectonic evolution of this area and partly by different interpretations of geochemical data. In this paper, we propose a new model based on analyses of the geochemistry of the CVRT in combination with results of previous studies.

GEOLOGICAL SETTING

Located on the northeast edge of the collision zone between the Indian and Eurasian plates, Tengchong is tectonically complex (Fig. 1). The Indian and Eurasian plates collided during the Early Cenozoic, which produced compressional structures in southern Tibet (Gansser 1981; Tapponier *et al.* 1981) and extensional structures in southeastern Asia (Tapponier *et al.* 1982). Consequently, post-collisional magmatism occurred along major tectonic zones and volcanism was active in rift zones or basins during the Cenozoic (Tapponier & Molnar 1977; Barr & Macdonald 1981; Chung *et al.* 1997). Several terranes can be distinguished in the surrounding areas of Tengchong such as Burma, Tengchong, Baoshan, and Simao (from west to east). Between these terranes there are three sutures: Myitkyina–Mandalay, Nujiang, and Lancangjiang (Jin 2002; Wang & Huangfu 2004).

Tengchong is usually interpreted as the southeastern part of the Himalayan belt (Wang *et al.* 2007). The basement of Tengchong is mainly composed of gneisses, migmatites, and migmatitic granites with minor mafic rocks exposed as small lenses (Chen *et al.* 2002). The basement is often considered to be the southeastern part of the Himalayan fold zone (Fan 1978; Powell & Johnson

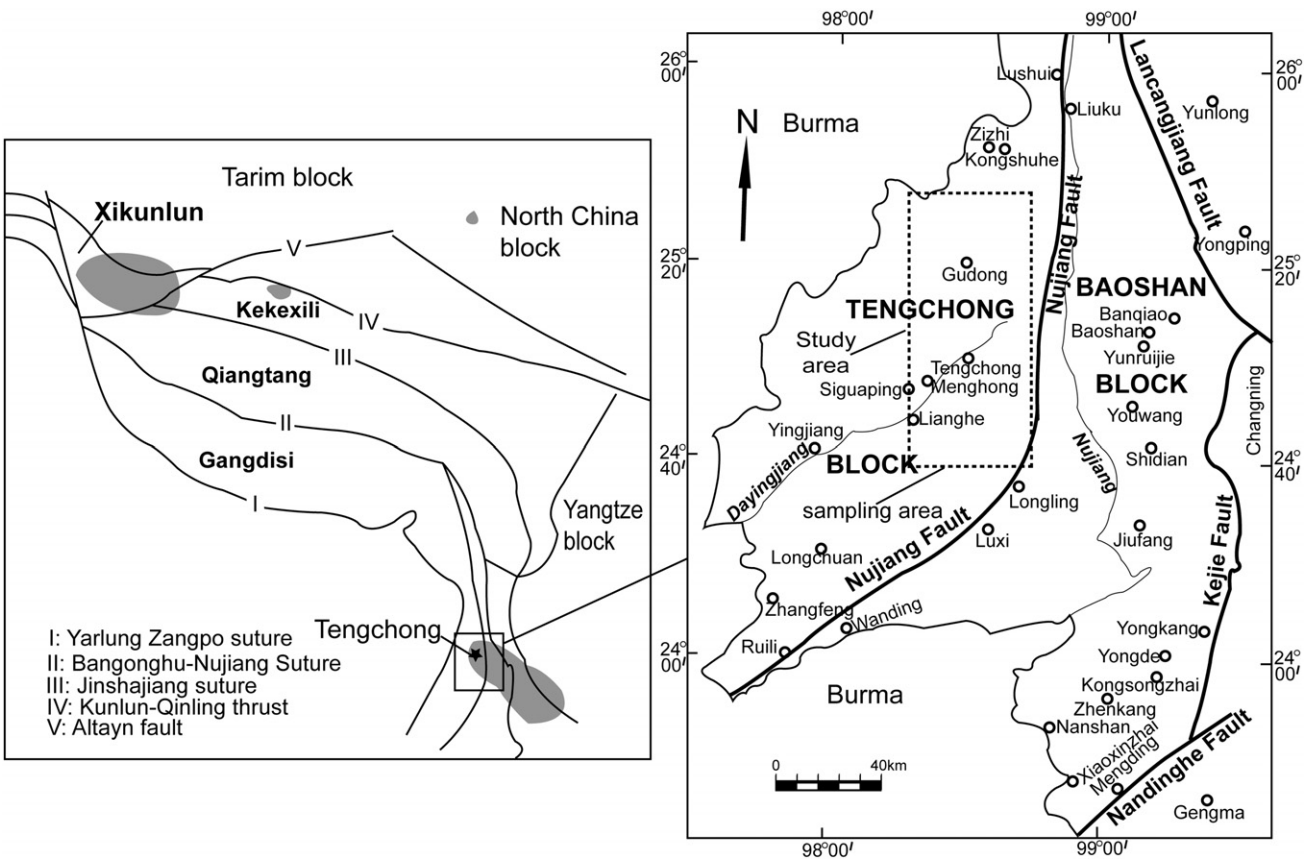

Fig. 1 Schematic map of Tengchong (right) and nearby area (left), showing main geological units, faults and place-names. Shaded areas in the left map indicate Cenozoic volcanic rocks as young as those in the CVRT.

1980) and is intruded by granitoids of late Mesozoic to Cenozoic age. To the east of Tengchong, there is the high-grade Proterozoic Gaoligong metamorphic zone (Yunnan Bureau of Geology and Mineral Resources 1979). Along the western side of Tengchong, late Mesozoic to early Cenozoic island-arc granites and gneisses are exposed between Burma and southwestern China (Yunnan Bureau of Geology and Mineral Resources 1979; Ji 1998; Jiang 1998). Sedimentary rocks of Tengchong form a roughly NS-trending belt in the centre of the block. The Permo-Carboniferous sequence constitutes most of these sedimentary rocks, which is composed of the clastic Menghong Group and the overlying carbonate-rich Dadongchang Group.

The Tengchong volcanic field is located within a NS-trending fault zone (Fig. 2) with lava flow coverage of more than 1000 km^2. Within this field, island-arc granites intruded into Mesozoic and Cenozoic geological units which represent the subduction of the Indian plate under the Eurasian plate along Naga Hills and Myitkyina–Mandalay suture zones (Ji 1998). According to Jiang (1998), the CVRT can be subdivided into four stages: Pliocene, early Pleistocene, late Pleistocene and Holocene. Most of these volcanic rocks are basaltic to andesitic in composition and are high-K calc-alkaline.

SAMPLING AND PETROLOGY

In order to have a clear notion of the spatial and geochemical evolution of the CVRT, samples were gathered from a vast area (Fig. 2). Twenty-five fresh samples (from 22 different locations) were collected (Table 1). These 25 samples belong to four groups which have different ages. Group 1 is Pliocene (N_2) in age and has six samples, Group 2 is early Pleistocene (Q_1) with five samples, Group 3 is late Pleistocene (Q_3) with six samples and Group 4 is Holocene (Q_4) with eight samples. Three rock types can be distinguished: basalt, andesite, and dacite. Most of these rocks (20 samples) are andesite whereas the remaining five samples are composed of basalts (two pieces) and dacites (three pieces). We made optical slices from fifteen samples and scrutinized them under a polarizing light microscope. Basalts have massive, vesicular or amygdaloidal structures and are dark in color, with porphyritic texture which has phenocrysts of plagioclase, clinopyroxene, and olivine. The groundmass consists of fine-grained to aphanitic minerals and opaque oxides. Andesites are grey in color and

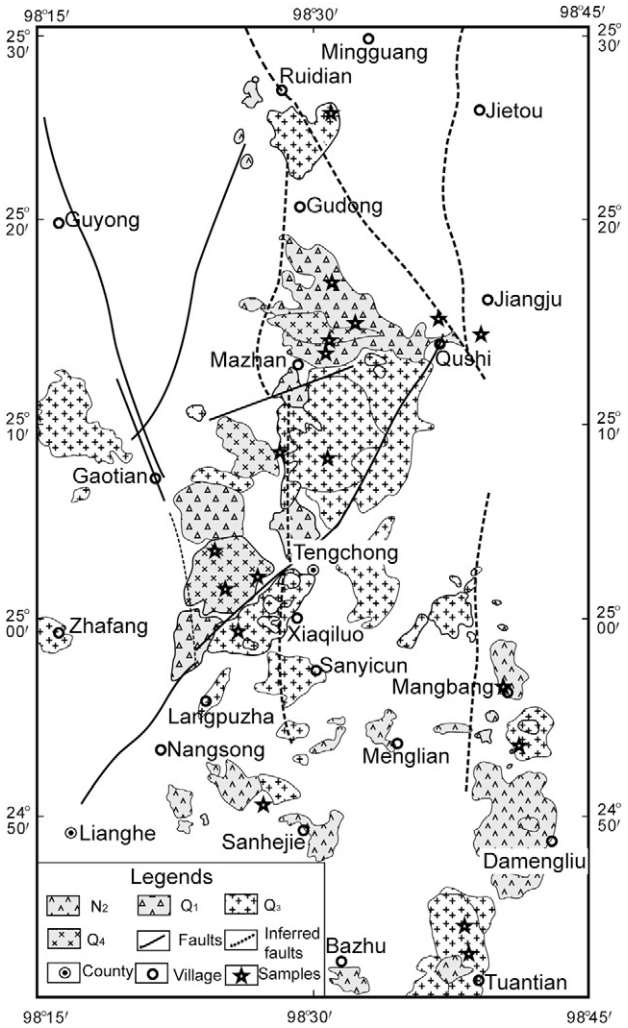

Fig. 2 Distribution of four stages of Cenozoic volcanic rocks in Tengchong and sampling locations. Abbreviations: N_2–Pliocene, Q_1–early Pleistocene, Q_3–late Pleistocene, Q_4–Holocene.

have massive and vesicular structures. These andesites are porphyritic and have phenocrysts of plagioclase, hornblende, and clinopyroxene. The groundmass of andesites is cryptocrystalline or glassy. Dacites are porphyritic in texture and have phenocrysts of plagioclase, quartz, orthoclase, etc. According to the electron probe micro-analyzer (EPMA) data, most of the plagioclases and clinopyroxenes of the CVRT are labradorite and augite, respectively, whereas augite and most olivine's Fo contents range from 71 to 79. (unpubl. data).

ANALYTICAL METHODS

Geochemical analyses were all performed at the Institute of Geology and Geophysics, Chinese Academy of Sciences (IGGCAS). Rock samples

Table 1 Location and rock types of Cenozoic volcanic rocks in Tengchong

No.	Sample name	Location	Rock types	Age
1	CQ08-1	N25°13′50.0″E98°37′50.0″	Basaltic trachyandesite	Q4
2	DY08-1	N25°07′30.5″E98°28′18.0″	Trachyandesite	Q4
3	GD08-1	N25°18′44.1″E98°29′01.7″	Basaltic trachyandesite	Q4
4	HT08-1	N25°10′51.7″E98°28′47.1″	Basaltic trachyandesite	Q4
5	LG08-3	N25°02′22.3″E98°25′54.3″	Basaltic trachyandesite	Q4
6	MA08-2	N25°01′18.0″E98°25′59.9″	Trachyandesite	Q4
7	MA08-3	N25°01′18.0″E98°25′59.9″	Trachyandesite	Q4
8	XC08-1	N25°02′05.9″E98°23′48.6″	Trachyandesite	Q4
9	CZ08-1	N25°14′06.8″E98°31′20.4″	Basaltic trachyandesite	Q3
10	CZ08-2	N25°14′06.8″E98°31′20.4″	Basaltic trachyandesite	Q3
11	HS08-1	N25°16′56.0″E98°28′39.7″	Trachyandesite	Q3
12	JS08-2	N25°13′39.9″E98°28′34.1″	Basaltic trachyandesite	Q3
13	JS08-3	N25°13′39.9″E98°28′34.1″	Basaltic trachyandesite	Q3
14	TS08-1	N25°14′02.8″E98°28′18.0″	Trachyandesite	Q3
15	BH08-1	N25°06′27.7″E98°32′54.1″	Dacite	Q1
16	LW08-3	N25°03′09.0″E98°32′45.5″	Dacite	Q1
17	TT08-2	N24°45′13.3″E98°37′47.7″	Trachyandesite	Q1
18	TT08-4	N24°44′29.3″E98°38′29.9″	Trachyandesite	Q1
19	YW08-2	N25°24′55.5″E98°30′02.9″	Dacite	Q1
20	DP08-1	N25°07′43.4″E98°28′12.1″	Trachyandesite	N2
21	HY08-1	N25°13′26.4″E98°34′43.4″	Basaltic trachyandesite	N2
22	MB08-1	N24°55′37.8″E98°40′10.0″	Basalt	N2
23	TT08-6	N24°40′53.0″E98°39′05.0″	Trachybasalt	N2
24	WH08-2	N24°53′06.1″E98°39′34.2″	Basalt	N2
25	XY08-1	N25°12′43.5″E98°34′41.1″	Basaltic trachyandesite	N2

were crushed and powdered to 200 mesh size in an agate mill. Major element analysis was carried out using X-ray fluorescence spectrometry (XRF) on fused glass disks. The precision and accuracy of the major-element data of the Chinese whole-rock basalt standard GSR-3 (Xie *et al*. 1989) are ≤3% and c. 5% (2σ), respectively. The FeO concentration was determined using conventional titration procedure and the error is less than 5%.

Trace element concentrations were measured by inductively coupled plasma mass spectrometry (ICPMS) with a Finnigan MAT Element II mass spectrometer. Samples were digested with a mixture of HF and HNO_3 acids in screw-top PTFE-lined stainless steel bombs at 185°C for two days, and insoluble residues were dissolved in HNO_3 acid heated to 145°C for 3 hours. Closed high-pressure bombs were used to ensure complete digestion. Precision for all trace elements is estimated to be 5% and accuracy is better than 5% for most elements, established through repeated analyses of the GSR-3 standard.

Sr–Nd–Pb isotopes were measured on a MAT 262 mass spectrometer. The Sr and Nd isotope ratios were normalized to $^{86}Sr/^{88}Sr = 0.1194$ and $^{146}Nd/^{144}Nd = 0.7219$. The La Jolla standard yielded $^{143}Nd/^{144}Nd = 0.511862 \pm 10$ (2 sigma, $n = 13$) and NBS-987 gave $^{87}Sr/^{86}Sr = 0.710240 \pm 11$ (2 sigma, $n = 6$). The $^{87}Rb/^{86}Sr$ and $^{147}Sm/^{144}Nd$ ratios were calculated using the Rb, Sr, Sm, and Nd abundances. Pb isotopic ratios were also obtained on the Finnigan MAT-262. Measured Pb isotopic ratios were corrected for instrumental mass fractionation of 0.1% per atomic mass unit by references to repeated analyses of the NBS-981 Pb standard. Repeated analyses of NBS-981 gave $^{204}Pb/^{206}Pb = 0.05897 \pm 15$, $^{207}Pb/^{206}Pb = 0.91445 \pm 80$, $^{208}Pb/^{206}Pb = 2.16170 \pm 180$ (2 sigma). Total blank levels were below 0.2 ng for Rb, Sr, and Nd, and around 0.5 ng for Pb.

ANALYTICAL RESULTS

MAJOR ELEMENTS

The result of the major element analysis is listed in Table 2. The loss of ignition (LOI) of these samples is small (less than 1.96 wt.%) except for YW08-2 (3.95 wt.%) which is probably due to high degree of alteration. The SiO_2 contents of these rocks have a range from 49.1 wt.% to 66.9 wt.%. TiO_2 contents are low and have a variation of 0.7 wt.%–1.6 wt.%, which is similar to those of island-arc volcanic rocks (McDermott & Hawkesworth 1991). The contents of TFe (sum of Fe_2O_3 and FeO) are not high (3.7 wt.%–10.0 wt.%), with most falling in the range of 5.4 wt.%–10.0 wt.%. Variation of Al_2O_3

Table 2 Whole rock major element compositions (wt.%) of Cenozoic volcanic rocks in Tengchong

Sample	SiO_2	TiO_2	Al_2O_3	Fe_2O_3	FeO	MnO	MgO	CaO	Na_2O	K_2O	P_2O_5	LOI	TOTAL
CQ08-1	51.57	1.60	17.11	2.58	7.06	0.16	6.67	7.29	3.58	1.89	0.38	0.44	100.33
DY08-1	62.04	1.09	16.31	1.81	3.68	0.09	2.51	4.59	3.63	3.99	0.39	0.06	100.19
GD08-1	55.38	1.21	16.29	1.87	5.69	0.13	5.98	7.14	3.43	2.42	0.27	0.44	100.23
HT08-1	54.73	1.51	17.35	2.38	5.61	0.13	4.89	7.09	3.94	2.60	0.43	–0.46	100.20
LG08-3	54.47	1.58	16.23	2.25	6.44	0.13	5.23	7.49	3.63	2.23	0.31	–0.30	99.70
MA08-2	59.05	1.29	16.73	2.07	4.27	0.11	3.61	5.64	3.88	3.25	0.46	0.02	100.36
MA08-3	58.73	1.25	16.51	1.63	4.68	0.11	3.55	5.57	3.83	3.36	0.45	0.06	99.72
XC08-1	58.55	1.30	16.72	1.98	4.43	0.11	3.71	5.73	3.82	3.17	0.46	0.08	100.06
CZ08-1	54.03	1.35	16.87	2.13	5.18	0.13	5.91	6.46	3.84	3.23	0.55	0.10	99.77
CZ08-2	54.28	1.36	16.88	1.99	5.29	0.13	5.81	6.65	3.91	3.21	0.55	–0.18	99.87
HS08-1	58.81	1.08	17.10	1.82	4.14	0.10	3.38	5.75	3.30	3.11	0.29	0.82	99.70
JS08-2	55.06	1.37	17.25	1.68	6.08	0.13	4.88	6.89	3.73	2.58	0.31	0.24	100.21
JS08-3	55.39	1.37	17.14	1.97	5.71	0.12	4.79	6.96	3.78	2.60	0.31	–0.12	100.03
TS08-1	58.93	1.21	16.55	1.91	4.36	0.11	4.06	5.92	3.63	3.25	0.43	0.00	100.36
BH08-1	66.92	0.66	15.38	1.20	2.65	0.07	1.79	3.97	3.47	3.61	0.18	0.12	100.01
LW08-3	66.69	0.69	15.96	2.31	1.43	0.06	0.94	3.34	3.27	3.66	0.22	1.02	99.59
TT08-2	62.05	1.02	16.21	2.49	2.90	0.10	2.76	5.03	3.62	3.25	0.38	0.38	100.17
TT08-4	61.24	1.06	16.43	2.51	3.03	0.09	2.92	5.23	3.35	3.43	0.39	0.50	100.18
YW08-2	62.12	0.93	17.97	1.89	4.91	0.08	1.92	0.76	0.91	4.13	0.13	3.95	99.71
DP08-1	61.25	1.11	16.33	1.38	4.24	0.09	2.68	4.87	3.71	3.78	0.40	–0.04	99.82
HY08-1	56.04	1.26	16.63	2.14	5.48	0.12	4.90	6.65	3.54	2.84	0.25	0.40	100.24
MB08-1	49.25	1.39	16.66	3.65	5.37	0.16	8.11	7.61	2.89	1.96	0.50	1.96	99.52
TT08-6	49.08	1.33	16.21	2.73	7.15	0.15	8.22	8.11	3.53	1.68	0.38	0.86	99.42
WH08-2	49.53	1.43	15.82	3.59	6.39	0.15	8.14	8.89	3.03	1.51	0.45	1.02	99.94
XY08-1	50.91	1.61	16.98	2.89	6.47	0.15	5.18	8.56	3.78	1.93	0.36	1.00	99.82

is also not large (15.4 wt.%–18.0 wt.%). MgO has a large variation (0.9 wt.%–8.2 wt.%). The total alkali contents have a range of 4.5 wt.% to 7.6 wt.%. Na_2O contents of nineteen samples are higher than K_2O contents with Na_2O/K_2O ratios of 1.06 (HS08-1) to 2.11 (TT08-6). Na_2O contents of the rest six samples are lower than K_2O contents with Na_2O/K_2O ratios of 0.22 (YW08-2) to 0.98 (DP08-1). As to P_2O_5 contents, all samples have similar values except YW08-2 and BH08-1, which have relatively low P_2O_5 contents.

In the total alkali *vs* SiO_2 (TAS) diagram (Fig. 3), five samples (CZ08-2, HT08-1, TT08-6, XY08-1, and CQ08-1) are ~~identified as~~ alkaline rocks and the rest 20 are sub-alkaline ones. In Figure 3, all the samples fall within the region enclosed with a solid line defined by former studies, indicating that they have similar rock types. Among the 20 sub-alkaline rocks, most are high-K calc-alkaline (consistent with the results of Xiang *et al*. 2000), and several samples fall into the shoshonite area (CZ08-1) or fall between high-K calc-alkaline and shoshonite areas (YW08-2, DY08-1, MA08-3, DP08-1, and MB08-1) (Fig. 4). In the alkalis-FeO-MgO (AFM) diagram (Fig. 5), 19 of the 20 sub-alkaline samples drop into the calc-alkaline area with the remaining sample (early Pleistocene YW08-2) drops into the tholeiitic area.

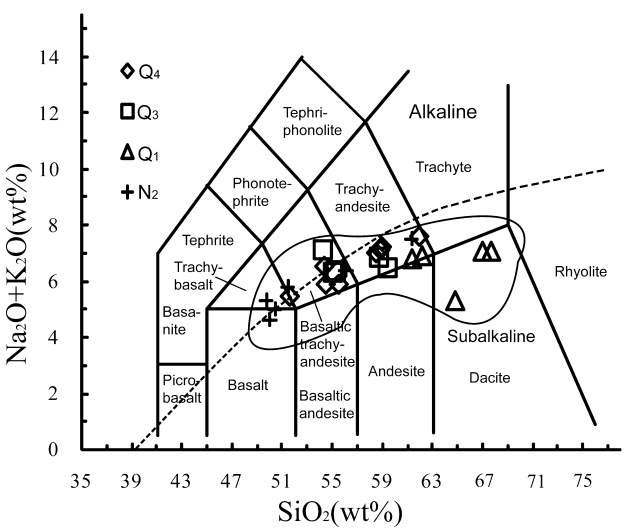

Fig. 3 Total alkali *vs* SiO_2 (TAS) diagram of the Cenozoic volcanic rocks in Tengchong. The broken line between alkaline and subalkaline areas comes from Irvine and Baragar (1971). All samples are enclosed by the solid line defined by the former studies of the Cenozoic volcanic rocks in Tengchong (reference data from Fan *et al*. 1999 and Xiang *et al*. 2000). ◊, Q_4; □, Q_3; △, Q_1; +, N_2.

As discussed above there are four groups of volcanic rocks in the CVRT: Group 1 is composed of basalt and andesite; Group 2 is composed of basalt, andesite, and dacite; Group 3 and Group 4 are both composed of andesite.

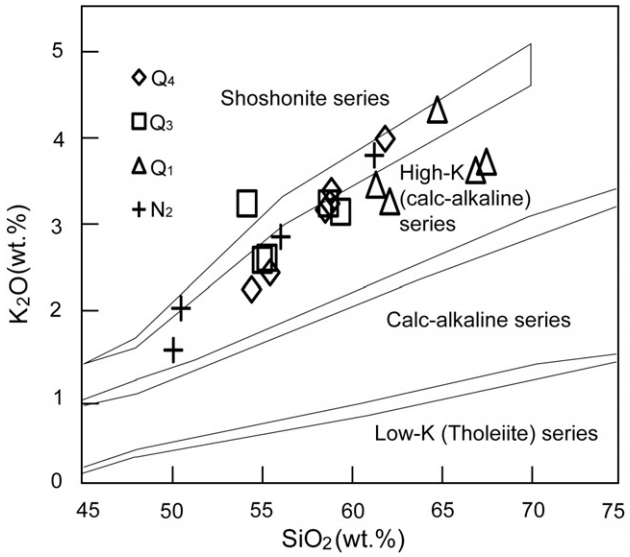

Fig. 4 K_2O (wt.%) *vs* SiO_2 (wt.%) classification diagram of the Cenozoic volcanic rocks in Tengchong indicating that most samples are plotted into high-K calc-alkaline series. Discrimination bands encircled by solid lines are after Rickwood (1989). ◊, Q_4; □, Q_3; △, Q_1; +, N_2.

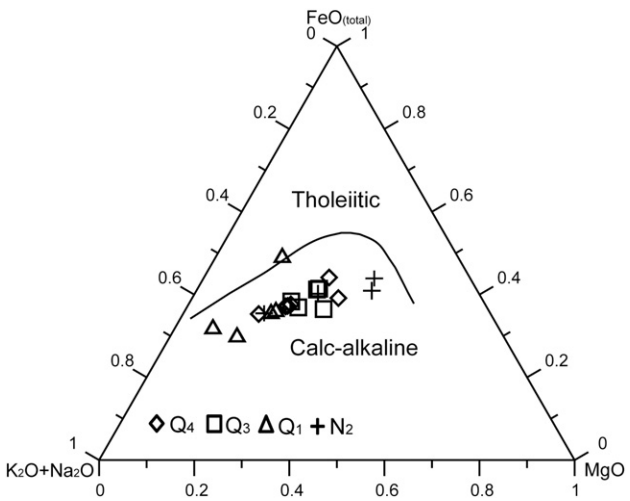

Fig. 5 AFM diagram of Cenozoic volcanic rocks in Tengchong showing most samples are calc-alkaline. The line between tholeiitic and calc-alkaline series is from Irvine and Baragar (1971). ◊, Q_4; □, Q_3; △, Q_1; +, N_2.

TRACE ELEMENTS

The results of trace element analyses are listed in Table 3. Transitional metallic elements such as Cr (3.9 ppm–221.9 ppm) and Ni (2.5 ppm–122.6 ppm) are low in contents and the total contents of rare earth elements (REE) have large variations (157 ppm–356 ppm). The REE contents obtained in this study are almost the same as those (151 ppm–326 ppm) from Zhou *et al.* (2000). Trace element ratios of these samples have large variations. For example, ratios of Nb/U, Ce/Pb, Nb/La, Ba/Nb, Rb/Nb, Th/Nb, Th/La, Ba/La and Rb/Sr are 3.86–21.66, 3.87–9.69, 0.23–0.66, 19.54–50.55, 0.43–3.88, 0.46–2.82, 0.18–0.64, 8.70–15.37 and 0.02–1.55, respectively.

All samples are enriched in light rare earth elements (LREE) and depleted in heavy rare earth elements (HREE) with the early Pleistocene rocks having the largest (LW08-3) and the Holocene rocks having the smallest (CQ08-1) fractionations between La and Yb [$(La/Yb)_N = 23.5$ and 8.44, respectively)]. Negative Eu anomalies are not conspicuous for most samples(>0.60). However, several samples have rather obvious Eu anomalies, among which BH08-1 has the smallest value (0.52). In the chondrite normalized REE distribution diagrams (Fig. 6), samples of all the four groups have very similar right oblique patterns with most samples having slight Eu anomalies. There are, however, subtle differences among the REE patterns of these four groups. For instance, the Eu anomalies of Group 2 (average $(Eu/Eu^*)_N$ is 0.63) are smaller than those of the other three groups (0.87, 0.73 and 0.76 for Group 1, Group 3 and Group 4), which can be used as a proof that Group 1 is more primary and did not experience strong fractionation of plagioclase. Another difference is that the LREE patterns of Group 1 and Group 4 show large variations compared with those of the other two groups.

In the primitive mantle normalized incompatible elements spider diagrams (Fig. 7), samples of all the four groups have similar right oblique patterns and share the following traits: enrichment in large ion lithophile elements (LILE) such as Rb and K; depletion of HREE and Y; obvious negative Nb-Ta anomalies and negative Sr-P anomalies, positive anomalies of Th, Pb and Nd. There are also differences among these four groups: the negative Nb-Ta anomalies of Group 1 and Group 2 are more conspicuous than those of the other two groups; the patterns of Group 4 highly resemble each other compared with the other three groups which have small differences among their distribution patterns. Also, the concentration patters in the chondrite normalized REE distribution diagrams (Fig. 6), and in the primitive mantle normalized multi-element concentration diagrams (Fig. 7), are similar to those of Zhou *et al.* (2000).

ISOTOPES

Sr-Nd-Pb isotope analyses were performed on eleven samples and the results are listed in Table 4.

Table 3 Whole rock trace element compositions (ppm) of Cenozoic volcanic rocks in Tengchong

Elements	CQ08-1	DY08-1	GD08-1	HT08-1	LG08-3	MA08-2	MA08-3	XC08-1	CZ08-1	CZ08-2	HS08-1	JS08-2	JS08-3	TS08-1	BH08-1	LW08-3	TT08-2	TT08-4	YW08-2	DP08-1	HY08-1	MB08-1	TT08-6	WH08-2	XY08-1
Sc	23.89	14.47	22.78	20.76	22.62	14.31	15.19	15.88	20.13	20.50	14.93	21.24	21.04	16.55	11.02	9.51	13.19	13.22	17.00	13.79	20.33	24.99	24.08	25.02	26.97
V	133.4	93.59	140.0	148.1	151.6	102.4	109.5	112.4	139.1	144.2	108.0	139.9	139.0	114.7	66.93	60.46	94.25	99.68	151.5	96.85	115.5	154.5	157.6	158.5	178.6
Cr	158.0	19.46	179.3	55.53	139.1	59.50	62.09	67.70	115.2	114.4	47.98	97.01	92.83	63.25	26.40	3.92	48.84	48.34	107.57	21.90	114.8	162.1	210.5	221.9	93.68
Co	33.85	13.60	28.93	27.29	30.41	16.23	17.27	18.08	27.05	27.63	17.29	28.02	27.20	19.53	8.37	6.99	13.66	13.70	21.80	14.72	25.59	34.55	39.61	41.21	30.43
Ni	53.85	20.33	73.73	38.83	43.70	29.10	30.91	35.68	84.32	82.29	40.33	40.87	42.09	54.07	9.17	2.47	16.42	14.29	50.02	23.78	34.45	107.2	122.6	120.0	30.40
Cu	22.79	19.87	28.52	21.74	28.94	19.65	20.17	23.15	28.99	27.61	22.47	26.08	25.82	22.38	12.28	9.07	14.67	14.91	10.88	18.23	22.49	31.72	32.01	30.77	30.55
Zn	93.30	82.33	82.20	91.85	97.13	77.96	81.76	88.34	76.77	76.41	83.47	82.40	82.23	85.63	63.56	62.37	92.03	86.45	91.97	81.73	83.71	75.99	87.27	91.55	83.45
Rb	35.20	132.2	80.29	66.14	68.39	93.70	98.90	97.89	86.42	87.08	109.6	69.20	69.22	99.24	157.4	156.8	94.79	88.12	176.6	128.2	83.72	36.88	37.53	21.46	38.79
Sr	424.0	443.5	450.2	537.5	417.3	491.9	513.5	550.5	705.6	734.7	483.8	422.7	436.7	517.9	314.0	320.2	563.7	581.6	113.7	483.8	355.1	656.8	733.6	930.3	510.0
Y	25.51	30.33	23.15	26.52	25.88	25.28	26.81	27.28	25.48	25.64	24.68	24.98	25.33	25.97	19.95	21.84	25.38	25.48	28.21	28.95	25.97	23.44	21.05	23.32	24.51
Zr	176.1	336.4	179.1	230.2	176.3	242.2	255.7	277.3	224.2	226.8	276.2	201.6	202.6	319.7	241.3	257.0	301.5	306.2	251.0	329.1	228.1	179.2	140.9	158.6	169.4
Nb	21.39	27.71	16.78	25.32	18.42	25.63	26.48	27.68	32.30	32.45	20.62	21.50	21.37	27.25	15.19	16.44	23.09	23.32	18.94	28.43	22.56	21.51	15.97	17.10	18.80
Cs	0.14	2.05	1.52	0.55	1.45	1.73	1.83	1.83	0.65	0.64	1.70	1.30	1.34	1.41	3.99	3.27	1.58	1.57	20.18	2.12	1.47	0.40	1.21	0.57	0.30
Ba	418.0	923.4	523.1	654.1	432.4	727.9	776.3	839.4	982.1	1002	822.8	441.6	448.8	966.0	585.0	638.1	977.3	1022	625.3	949.9	476.4	821.8	592.1	864.2	484.3
La	32.35	83.31	45.08	50.50	38.66	65.45	65.10	67.47	69.27	68.55	75.99	42.74	43.67	71.41	67.23	72.53	76.97	81.40	51.60	80.86	49.32	53.48	41.68	61.72	34.42
Ce	62.00	158.9	84.69	94.17	73.98	124.5	121.3	128.9	124.3	131.3	154.9	80.71	81.28	141.3	136.9	130.3	144.5	148.7	101.6	160.9	89.48	94.74	74.79	112.8	67.89
Pr	7.43	16.98	9.65	10.95	8.73	13.55	13.54	14.27	13.41	14.19	16.94	9.29	9.34	15.10	15.71	16.38	15.53	16.39	12.23	17.52	9.87	10.69	8.41	13.42	7.90
Nd	28.65	61.81	36.08	41.00	32.85	47.25	49.06	52.81	47.76	49.84	63.06	33.87	34.65	54.24	57.58	59.04	54.71	56.81	45.52	62.86	35.81	39.40	31.66	50.30	30.42
Sm	5.77	9.55	6.05	7.01	5.96	7.59	7.97	8.69	7.93	7.96	9.47	5.95	6.11	8.88	8.51	9.08	8.48	9.18	8.01	9.70	6.28	6.44	5.44	7.96	5.79
Eu	1.76	1.82	1.38	1.81	1.65	1.60	1.72	1.96	1.93	1.82	1.73	1.47	1.48	1.91	1.31	1.61	2.00	1.83	1.47	1.94	1.41	1.96	1.77	2.29	1.69
Gd	5.72	7.90	5.24	6.33	5.77	6.25	6.48	6.97	6.66	6.65	7.63	5.54	5.55	7.20	6.41	6.82	6.97	7.32	6.73	7.98	5.49	5.68	5.03	6.37	5.40
Tb	0.92	1.07	0.80	0.94	0.91	0.91	0.97	1.02	0.91	0.92	0.98	0.81	0.84	0.99	0.87	0.92	0.96	1.00	1.02	1.08	0.85	0.85	0.77	0.91	0.87
Dy	5.39	5.82	4.45	5.29	5.32	4.95	5.37	5.62	4.84	4.98	5.07	4.73	4.86	5.43	4.25	4.84	5.23	5.57	5.88	5.83	5.01	4.93	4.43	5.06	5.17
Ho	1.10	1.14	0.91	1.07	1.08	0.96	1.05	1.12	0.98	0.95	0.94	0.97	0.98	1.00	0.82	0.90	1.02	1.06	1.17	1.10	0.99	1.01	0.91	1.01	1.10
Er	2.91	3.04	2.48	2.81	2.90	2.59	2.82	3.08	2.60	2.65	2.46	2.58	2.63	2.72	2.14	2.30	2.66	2.78	3.27	2.96	2.75	2.70	2.40	2.69	2.77
Tm	0.41	0.42	0.36	0.41	0.39	0.38	0.41	0.42	0.38	0.39	0.34	0.37	0.39	0.39	0.31	0.32	0.40	0.39	0.50	0.42	0.41	0.38	0.35	0.38	0.40
Yb	2.58	2.65	2.31	2.56	2.45	2.49	2.61	2.69	2.46	2.46	2.19	2.37	2.47	2.44	1.96	2.08	2.45	2.47	3.22	2.62	2.60	2.40	2.14	2.32	2.51
Lu	0.38	0.42	0.35	0.38	0.37	0.38	0.40	0.42	0.35	0.37	0.32	0.35	0.36	0.37	0.28	0.32	0.38	0.36	0.50	0.39	0.39	0.36	0.32	0.35	0.37
Hf	4.45	8.53	4.74	5.74	4.72	6.10	6.60	7.33	5.52	5.54	7.67	5.11	5.07	8.03	7.14	7.36	7.83	7.91	7.36	8.59	5.90	4.33	3.66	3.96	4.25
Ta	1.30	1.72	1.05	1.49	1.15	1.53	1.63	1.71	1.86	1.92	1.33	1.32	1.33	1.65	1.18	1.21	1.43	1.43	1.43	1.75	1.38	1.21	0.94	0.96	1.13
Pb	7.47	27.67	14.51	11.69	11.40	18.26	19.29	20.58	13.89	13.55	24.03	13.15	13.06	19.37	31.12	33.68	26.32	24.59	19.46	24.64	15.33	12.39	8.61	12.24	8.45
Th	9.83	32.77	20.67	15.25	16.48	23.16	22.97	24.09	21.40	21.67	34.16	18.70	19.47	23.28	42.78	35.62	22.81	22.84	19.71	34.30	23.03	12.84	9.90	11.36	10.15
U	1.10	3.21	2.04	1.67	1.65	2.41	2.60	2.68	2.46	2.46	2.81	1.88	1.91	2.49	3.93	3.96	2.52	2.50	2.58	3.09	2.05	1.65	1.44	1.43	0.87

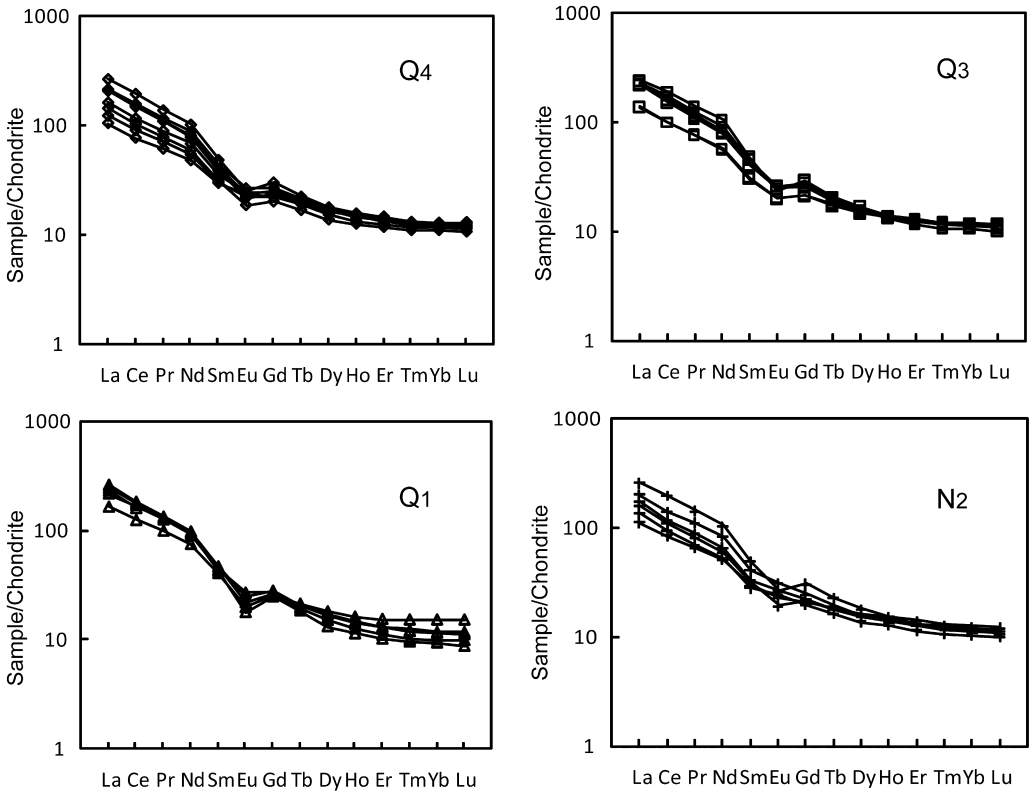

Fig. 6 Chondrite-normalized REE patterns for Cenozoic volcanic rocks in Tengchong. Rocks from the four stages have similar patterns and slightly negative Eu anomalies. Normalization values of chondrite come from Boynton (1984).

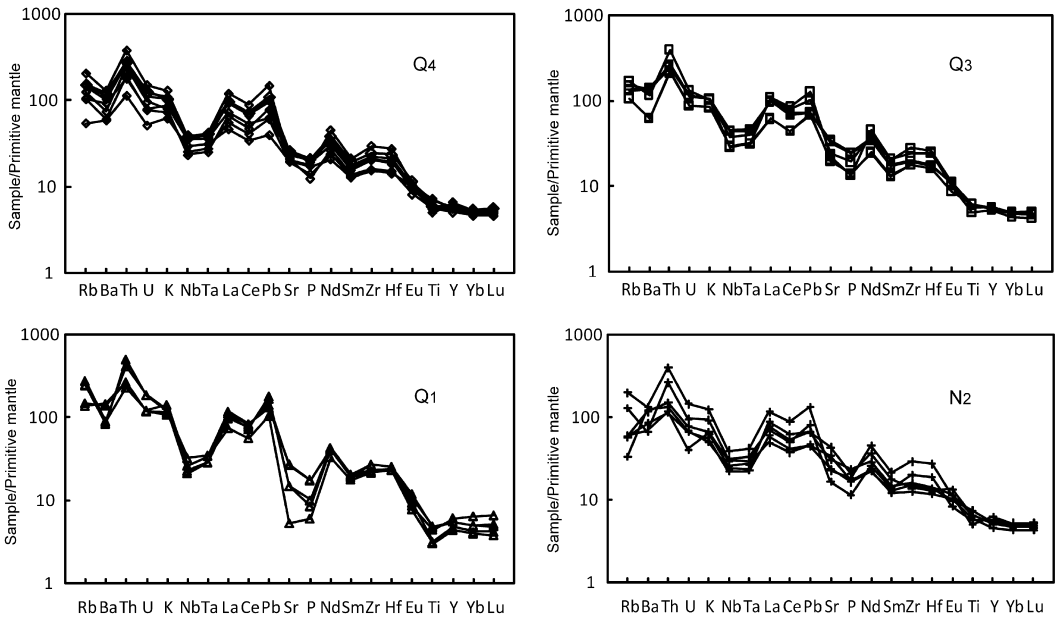

Fig. 7 Primitive-mantle normalized trace element patterns for the Cenozoic volcanic rocks in Tengchong. Rocks from the four stages have similar distribution shape and negative Nb-Ta anomalies. Normalization values of primitive mantle come from Sun and Mcdonough (1989).

Of the 11 samples, three belong to the Pliocene (HY08-1, MB08-1, and WH08-2), two belong to the early Pleistocene (BH08-1 and TT08-1), one belongs to the late Pleistocene (JS08-3) and the rest five belong to the Holocene. Most samples have the following Sr-Nd isotope traits: $^{87}Sr/^{86}Sr$ ratios fall in the range of 0.7057–0.7093, while $^{143}Nd/^{144}Nd$ are higher than 0.5120 and εNd(0) values are all

Table 4 Sr-Nd-Pb isotope analyses of the Cenozoic volcanic rocks in Tengchong

Sample	CQ08-1	DY08-1	HT08-1	LG08-3	MA08-3	JS08-3	BH08-1	TT08-4	HY08-1	MB08-1	WH08-2
$^{87}Sr/^{86}Sr$	0.705749	0.708804	0.706792	0.706472	0.707535	0.705747	0.709301	0.708806	0.706220	0.708145	0.708252
2σ	12	12	11	9	11	12	10	10	12	10	10
$^{143}Nd/^{144}Nd$	0.512521	0.512189	0.512376	0.512371	0.512287	0.512362	0.512013	0.512272	0.512385	0.512402	0.512443
2σ	15	10	13	11	10	11	12	15	15	11	12
εNd(0)	–2.28	–8.76	–5.11	–5.21	–6.85	–5.38	–12.19	–7.14	–4.94	–4.60	–3.80
$^{206}Pb/^{204}Pb$	18.2766	18.0693	18.1597	18.1653	18.1303	18.1395	17.9356	18.2671	18.2202	18.0255	18.0652
2σ(M)%	0.009	0.011	0.012	0.018	0.011	0.013	0.009	0.009	0.009	0.013	0.007
$^{207}Pb/^{204}Pb$	15.6530	15.6556	15.6511	15.6617	15.6503	15.6476	15.6137	15.6671	15.6624	15.6385	15.6769
2σ(M)%	0.011	0.011	0.013	0.023	0.012	0.011	0.008	0.008	0.01	0.016	0.009
$^{208}Pb/^{204}Pb$	39.0851	39.1074	39.0514	39.1435	39.0904	39.0728	39.0888	39.1875	39.1336	38.8936	38.9835
2σ(M)%	0.012	0.011	0.015	0.027	0.013	0.015	0.009	0.009	0.011	0.018	0.015

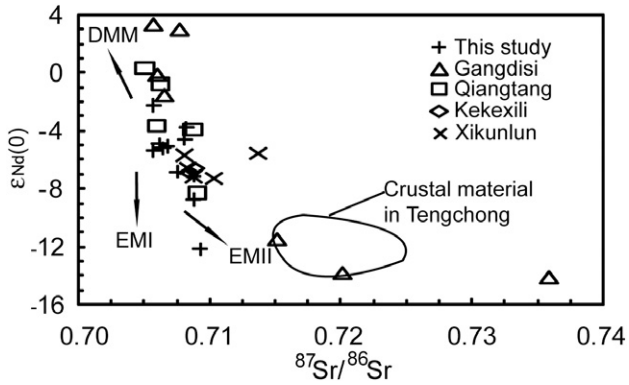

Fig. 8 εNd(0)-$^{87}Sr/^{86}Sr$ diagram for Cenozoic volcanic rocks in Tengchong. The distribution of CVRT overlaps much with those of Gangdisi and Qiangtang. Data of Gangdisi comes from Coulon *et al.* (1986), Arnaud *et al.* (1992), Miller *et al.* (1999) and Zhao *et al.* (2001). Data of Qiangtang come from Deng (1998), Deng and Sun (1998) and Ding *et al.* (1999). Data of Kekexili come from Turner *et al.* (1996), Deng (1998), Deng and Sun (1998) and Lai *et al.* (2001). Data of Xikunlun come from Arnaud *et al.* (1992), Xie *et al.* (1992), Deng (1998) and Deng and Sun (1998). Data of crustal material in Tengchong come from Chen *et al.* (2002). Enriched mantle I (EMI), enriched mantle II (EMII) and depleted mantle (DM) come from Zindler and Hart (1986). +, This study; △, Gangdisi; □, Qiangtang; ◊, Kekexili; ×, Xikunlun.

negative (–2.28 to –12.19). Lead isotope ratios are something like those of Sr-Nd isotopes. These samples have $^{206}Pb/^{204}Pb$ ratios of 17.936–18.277, $^{207}Pb/^{204}Pb$ ratios of 15.614–15.677 and $^{208}Pb/^{204}Pb$ ratios of 38.894–39.188, respectively.

The isotopic data of the CVRT are plotted in Figures 8 and 9. In these figures, the isotopic data of the Cenozoic volcanic rocks in Gangdisi (Coulon *et al.* 1986; Arnaud *et al.* 1992; Miller *et al.* 1999; Zhao *et al.* 2001), Qiangtang (Deng 1998; Deng & Sun 1998; Ding *et al.* 1999), Kekexili (Turner *et al.* 1996; Deng 1998; Deng & Sun 1998; Lai *et al.* 2001) and Xikunlun (Arnaud *et al.* 1992; Xie *et al.* 1992; Deng 1998; Deng & Sun 1998) from the Tibetan Plateau and its margin are also plotted. Rocks from Gangdisi have the largest distribution range, with the maximum εNd(0) and $^{87}Sr/^{86}Sr$ values. The Sr-Nd distribution of the CVRT overlaps with much of that of the Gangdisi and Qiangtang rocks. However, because the lead isotopic data of the CVRT do not overlap with those of the other regions (see Fig. 9), the geochemical features of the source mantle beneath Tengchong are different from those beneath the other regions. The Sr and Nd isotopic data of the CVRT are distinguishable from those of crustal rocks in Tengchong (Chen *et al.* 2002), implying not very severe crustal contamination. In Figure 9, rocks from Qiangtang have the largest lead isotope ratio variations. Unlike the Sr-Nd traits, the CVRT do not overlap

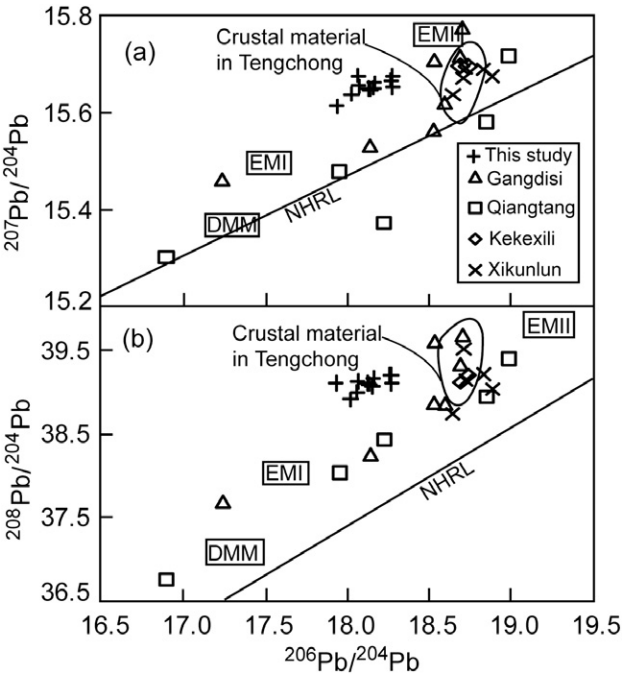

Fig. 9 $^{207}Pb/^{204}Pb(t)$-$^{206}Pb/^{204}Pb(t)$ (a) and $^{208}Pb/^{204}Pb(t)$-$^{206}Pb/^{204}Pb(t)$ (b) diagrams for the Cenozoic volcanic rocks in Tengchong. CVRT do not overlap with those from other four regions, indicating their source region is unique in lead isotopes. The reference date are the same as Figure 8. EMI and EMII come from Zindler and Hart (1986). NRHL stands for north hemisphere reference line which has Th/*U*-value of 4.0 in (a) and the slope of which has an age significance of 1.77 Ga in (b).

with those from the other four regions, indicating their source region is unique in lead isotopes and they inherited the lead isotope characteristics from their source region. Again, it is also clear that the CVRT data are significantly different from those of crustal rocks in Tengchong (Chen *et al.* 2002) in Figure 9.

DISCUSSION

PETROGENESIS

The low Ni (2.5 ppm–122.6 ppm) and Cr (3.9 ppm–221.9 ppm) contents and Mg-numbers (0.41–0.73) of these samples suggest that they experienced considerable crystal fractionation. Fractionation trends can be seen clearly in the Harker diagram (Fig. 10), in which negative correlations exist between TiO_2, $FeO + Fe_2O_3$, MgO, P_2O_5, CaO, and SiO_2, implying that minerals such as pyroxene, olivine, and apatite have fractionated before the emplacement of the basalts. The Al_2O_3 contents do not change much with the increase of SiO_2, indicating significant fractionation of plagioclase. This is because the effect of the increase in Al_2O_3 content by extensive fractionation of Al-free mafic phases is counterbalanced by the effect of the decrease in Al_2O_3 content by plagioclase fractionation.

The upper crust in Tengchong consists mainly of granites (most are Mesozoic in age) and the middle-lower crust consists partly of amphibolites (Chen *et al.* 2002). It is worth noting that crustal rocks can be ruled out as possible sources for the CVRT because experimental evidence shows that partial melting of any of the older crustal rocks (e.g. Hirajima *et al.* 1992; Yang *et al.* 1993; Zhang *et al.* 1994, 1995; Kato *et al.* 1997) and lower crustal intermediate granulites (Gao *et al.* 1998a, b) in the deep crust would produce high-Si, low-Mg liquids (e.g. granitoid liquids; Rapp *et al.* 2003), which is not the case for the CVRT.

Elevated SiO_2 contents, high $^{87}Sr/^{86}Sr$ ratios and low $\varepsilon Nd(0)$ values are commonly used as indicators of crustal contamination for mafic melts (DePaolo 1981). The wide range of SiO_2 content (49.1 wt.%–66.9 wt.%) (Fig. 3), high values of $^{87}Sr/^{86}Sr$ (0.7057–0.7093) (Fig. 8) and negative $\varepsilon Nd(0)$ values (–2.28 to –12.19) indicate that the CVRT probably have undergone different degrees of crustal contamination. The crustal contamination can also be distinguished in the $^{87}Sr/^{86}Sr$ *vs* MgO diagram (Fig. 11), in which the $^{87}Sr/^{86}Sr$ values decrease with the increment of MgO. That is to say, the primary magma has lower $^{87}Sr/^{86}Sr$ values and higher contents of MgO, and the magma was contaminated by the crustal materials with high $^{87}Sr/^{86}Sr$ values and low content of MgO. Geophysical observations (Qin *et al.* 2000; Jiang *et al.* 2004; Zhao *et al.* 2006) suggest that magma chambers are located in the crust at a depth of <20 km. Therefore, evolved magmas may have formed through assimilation and fractional crystallization in such crustal magma chambers.

Hart (1984) distinguished different mantle components using their radioactive isotopes such as Sr, Nd, and Pb. Sr-Nd-Pb isotopic compositions and the ratios of highly incompatible elements with similar bulk distribution coefficients (e.g. Th/La, Zr/Nb, Ce/Pb and Nb/U) are seldom affected in partial melting or crystal fractionation processes and, therefore, they are powerful tools in identifying the source region of the volcanic rocks. In Figures 8 and 9, the CVRT data can primarily be explained by the mixture of enriched mantle I (EMI), enriched mantle II (EMII), and depleted MORB-source mantle (DMM), although some data may be affected significantly by crustal assimilation as discussed above. Therefore, these three mantle

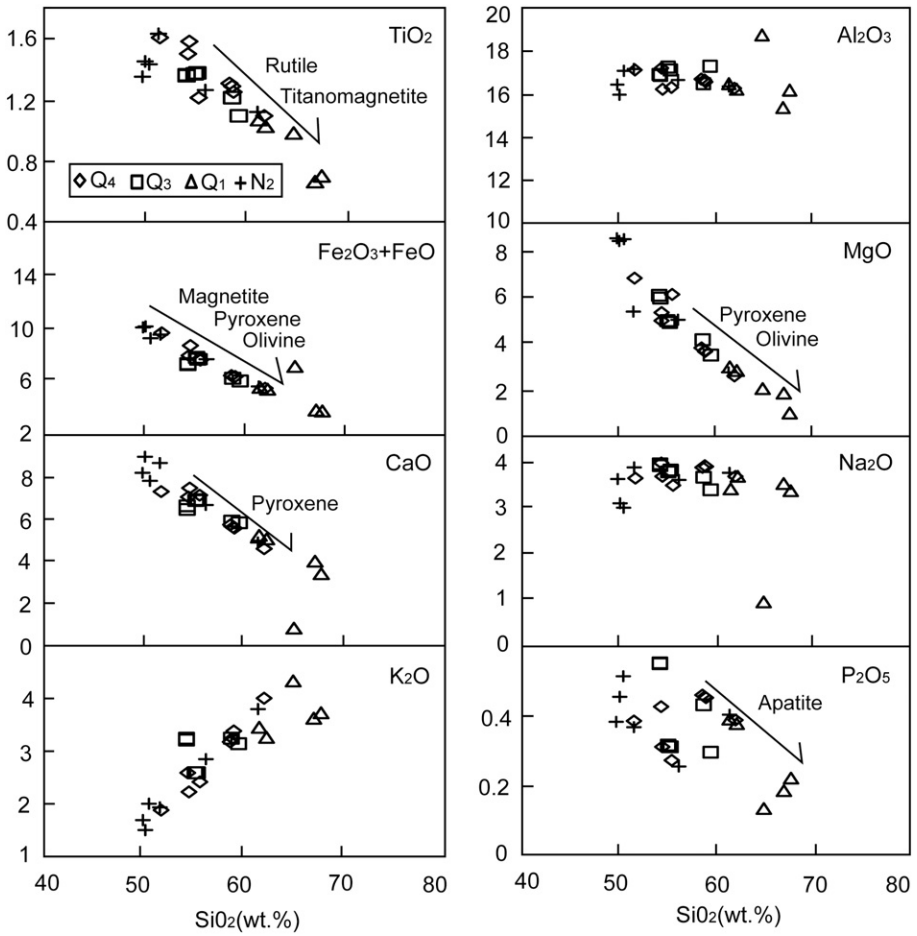

Fig. 10 Harker diagram of the Cenozoic volcanic rocks in Tengchong to evaluate fractionation trend. The probable fractionated minerals are shown above the arrows.

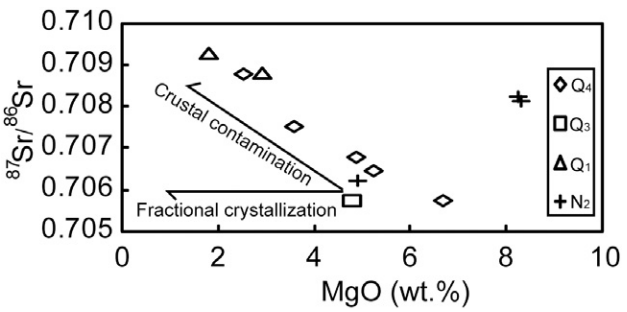

Fig. 11 $^{87}Sr/^{86}Sr$-MgO diagram of the Cenozoic volcanic rocks in Tengchong to evaluate probable crustal contamination.

components might have been involved in the generation of the CVRT magmas. Enrichment in LILE and LREE and the EMI- and EMII-rich characters of the CVRT magmas suggest that the source might have been in the lithospheric mantle.

For these considerations, the eruption of the CVRT can be summarized as follows: firstly, the primary magma formed in the lithospheric mantle, and rose rapidly into the crust to form a magma chamber, in which the magma experienced crystal fractionation and simultaneous assimilation of the wall rocks. Then, the magma erupted to the surface and formed the CVRT. This scenario can explain the geochemical characters of the CVRT (such as mantle-derived, crustal contamination and fractionation trend) and is in accord with the present observation of the magma chambers beneath Tengchong.

TECTONIC IMPLICATIONS

The low TiO_2 contents, obvious Nb-Ta negative anomalies and slightly enriched Sr-Nd-Pb isotope ratios of the CVRT are similar to those of island-arc rocks which have the above mentioned traits. Moreover, theses rocks include basalt, andesite and dacite, which are typical assemblages of island-arc rocks. However, the CVRT are obviously products of intraplate environments. So, why CVRT have island-arc imprints? Dating shows that the continental-continental collision (Fig. 12(a), (b)) completed at least at the end of the Cretaceous (about 65 Ma) in Tengchong. After the

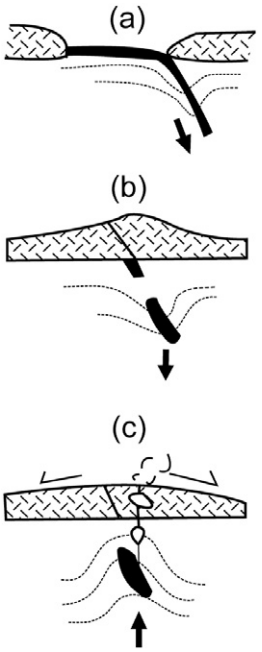

Fig. 12 Schematic diagrams illustrating the three stages in generating the Cenozoic volcanic rocks in Tengchong. Detailed meaning of these diagrams can be found in the text.

collision Tengchong was in an intraplate state. That is to say that the eruption of the CVRT (the oldest age of most of them is about 3.7 Ma) was later than the collision by about 65 Ma.

Within and around the Tibetan Plateau, Cenozoic volcanic rocks are widely exposed. But, volcanic rocks as young as those in Tengchong are scarce and are restricted to several places (Mo *et al.* 2006) such as to the northwest, southeast and northeast edges of the Tibetan Plateau. Because of their locations to the northwest and southeast edges of the Tibetan Plateau, which are near the west and east tectonic syntaxis, it is inferred that these volcanic rocks are linked with the evolution of the Tibetan Plateau. Wang *et al.* (2001) studied the Cenozoic volcanic activities in the eastern Indo-Asian collision zone and pointed out that the younger rocks are widely distributed in rift basins and are coeval with the east-west extension of Tibet and eastern Asia.

Mu *et al.* (1987) systematically measured the age of the CVRT and revealed that the main eruption age of the CVRT is 0–3.7 Ma. The uplift of the Tibetan Plateau is a scientific concern of many different realms. By the high-resolution magnetostratigraphy on the NE Tibetan Plateau, Fang *et al.* (2007) proposed that the Tibetan Plateau experienced at least three rapid uplifts which started at about 14.7 Ma, 8.1 Ma and 3.6 Ma. Thus, the eruption of the CVRT started almost synchronously with the 3.6 Ma rapid uplift of the Tibetan Plateau and some kind of link may exist between them. Meanwhile, Zhang *et al.* (2001) studied the structural-chronological frame of the eastern Himalayan syntaxis and found that it collapsed after about 6–7 Ma and thought the collapse represented a rapid uplift of the Tibetan Plateau.

After the final collision between the Burma and Tengchong terranes, the regional structural deformation style had transformed from the predominance of compression in the syn-tectonic stage into lithospheric extension during the post-orogenic stage because of the collapse of the collisional orogenic belt. For example, according to the study of Wang *et al.* (2007), extension and strike-slip were dominant structure types since about 6–4 Ma in Tengchong. Extensional tectonics in orogenic belts usually develop during the post-orogenic stage in response to readjustment of the lithospheric thinning by means of mantle convection, lithospheric collapse, slab breakoff, and/or detachment (England & Houseman 1989; Platt & England 1994; Ruppel 1995; Davis & Von Blanckenburg 1995). When the degree of extension is large enough to make the geotherm graze the solidus, decompressional melting will take place. According to the studies of Jiang *et al.* (2003), most CVRT occur in basins bordered by normal faults, indicating that these Cenozoic volcanic rocks formed in an extensional state, which is in accord with the above principle. That is to say, before the eruption of CVRT the extension of the Tengchong lithosphere had existed for a long time and when the extension was large enough, decompressional melting of the CVRT source region took place and the magma finally erupted to the surface.

Tengchong is a part of the eastern Himalayan syntaxis. According to the aforementioned interpretation of Zhang *et al.* (2001), the syntaxis collapsed as a result of the rapid uplift of the Tibetan Plateau. So, we propose that the uplift of the Tibetan Plateau caused the collapse of the collisional orogenic belt in Tengchong. Due to the decompression of the enriched lithospheric mantle which was caused by the collapse, the magma was generated and was stocked in the crust. After assimilation and fractional crystallization in magma chambers the evolved magmas erupted (Fig. 12(c)) and emplaced in basins bordered by normal faults. We also suggest that CVRT, which are classified as intraplate volcanism, have an island-arc signature because the source mantle was metasomatized by previous subduction events.

As mentioned in the introduction, many models have been put forward to explain the CVRT. Some of these models are consistent with our newly obtained geochemical data such as that the CVRT have island-arc imprints and that the source region is enriched mantle. However, these models are not sufficient to give us a clear conception of the formation of the CVRT. For example, the model of Zhu *et al.* (1983) and Mu *et al.* (1987) concerned only with the tectonic environment of the CVRT, models of Zhao and Chen (1992) and Cong *et al.* (1994) just considered that the CVRT are products of island-arc volcanism, the model of Ji (1998) merely pointed out the upwelling of the upper mantle in Tengchong and the model of Chen *et al.* (2002) concerned with the source region of the CVRT. Our model shares many similar characteristics with previous models such as island-arc prints (Zhu *et al.* 1983; Mu *et al.* 1987; Zhao & Chen 1992), enriched mantle source region (Chen *et al.* 2002) and upwelling of the upper mantle (Ji 1998). However, compared with previously proposed models concerning the CVRT, our model is unique in that it links the uplift of the Tibetan Plateau with the eruption of the CVRT for the first time.

CONCLUSIONS

The CVRT are mainly composed of basalt, andesite, and dacite and most of them are sub-alkaline and high-K calc-alkaline. Major, trace, and isotope geochemical characteristics of the CVRT resemble those of the volcanic rocks which erupted in an island-arc. Geochemical data of the CVRT suggest that the EMI-, EMII- and DMM-like components, which resided in the lithospheric mantle, probably involved in the magma genesis. Petrogenesis studies also show that the CVRT experienced assimilation and fractional crystallization (AFC) process. Considering the nearby tectonic evolution around Tengchong, we conclude that the uplift of the Tibetan Plateau caused the collapse of the collisional orogeny in Tengchong, which further triggered the generation of magma and the eruption of the CVRT.

ACKNOWLEDGEMENTS

This study was financially supported by China Petroleum & Chemical Corporation (SINOPEC) (No: YPH08064), National Science Found Committee (40803012), China Postdoctoral Science Foundation, Major State Basic Research Development Program of China (973) (No: 2009CB219301) and the Technology and Experiment of Deep Drilling (SinoProbe-05-03). Doctors Meng Q.Q and Zhu D.Y. are thanked for their assistance in field work.

REFERENCES

ARNAUD N. O., VIDAL P. H., TAPPONNIER P., MATTE P. H. & DENG W. M. 1992. The high K_2O volcanism of northwestern Tibet: Geochemistry and tectonic implications. *Earth and Planetary Science Letters* **111**, 351–67.

BAI D. H., LIAO Z. J. & ZHAO G. Z. 1994. Study on magmatic source of Rehai-Retian in Tengchong from MT investigating results. *Chinese Science Bulletin* **39**, 344–7 (in Chinese).

BARR S. M. & MACDONALD A. S. 1981. Geochemistry and geochronology of late Cenozoic basalts of southeast Aias. *Geological Society of America Bulletin* **92**, 1069–142.

BOYNTON W. V. 1984. Geochemistry of the rare earth elements: Meteorite studies. *In* Henderson P. (ed.) *Rare Earth Element Geochemistry*, pp. 63–114, Elsevier, Amsterdam.

CHEN F., SATIR M., JI J. & ZHONG D. 2002. Nd-Sr-Pb isotopes of Tengchong Cenozoic volcanic rocks from western Yunnan, China: Evidence for an enriched-mantle source. *Journal of Asian Earth Sciences* **21**, 39–45.

CHUNG S. L., LEE T. Y., LO C. H. *et al.* 1997. Intraplate extension prior to continental extrusion along the Ailao Shan-Red River shear zone. *Geology* **25**, 311–4.

CONG B. L., CHEN Q. Y., ZHANG R. Y., WU G. Y. & XU P. 1994. Petrogenesis of Cenozoic rocks in Tengchong region of western Yunnan Province, China. *Science in China (Series B)* **37**, 1264–71 (in Chinese).

COULON C., MALUSKI H., BOLLINGER C. & WANG S. 1986. Mesozoic and Cenozoic volcanic rocks from central and southern Tibet: ^{39}Ar-^{40}Ar dating, petrological characteristics and geodynamical significance. *Earth and Planetary Science Letters* **79**, 281–302.

DAVIS J. H. & VON BLANCKENBURG F. 1995. Slab breakoff: A model of lithosphere detachment and its test in the magmatism and deformation of collisional orogens. *Earth and Planetary Science Letters* **129**, 327–43.

DENG W. M. 1998. *Cenozoic Intraplate Volcanic Rocks in the North Tibet Plateau*. Geological Publishing House, Beijing (in Chinese).

DENG W. M. & SUN H. J. 1998. Isotopic geochemistry and source of intraplate volcanic rocks in north Tibet, China. *Earth Science Frontiers* **5**, 307–17. (in Chinese with English abstract).

DEPAOLO D. J. 1981. Trace element and isotopic effects of combined wall rock assimilation and fractional

crystallization. *Earth and Planetary Science Letters* **53**, 189–202.

DING L., ZHANG J. J., ZHOU Y., DENG W. M., XU R. H. & ZHONG D. L. 1999. Tectonic implication on the lithosphere evolution of the Tibetan Plateau: Petrology and geochemistry of sodic and ultrapotassic volcanism in Northern Tibet. *Acta Petrologica Sinica* **15**, 408–21 (in Chinese with English abstract).

ENGLAND P. C. & HOUSEMAN G. A. 1989. Extension during continental convergence, with application to the Tibet Plateau. *Journal of Geophysical Research* **94**, 17561–79.

FAN P. F. 1978. Outline of the tectonic evolution of the southwestern China. *Tectonophysics* **45**, 261–7.

FAN Q. C., LIU R. X., WEI H. Q. *et al*. 1999. The magmatic evolution of the active volcano in the Tengchong area. *Geological Review* **45**, 895–904.

FANG X. M., ZHANG W. L., MENG Q. Q. *et al*. 2007. High-resolution magnetostratigraphy of the Neogene Huaitoutala section in the eastern Qaidam Basin on the NE Tibetan Plateau, Qinghai Province, China and its implication on tectonic uplift of the NE Tibetan Plateau. *Earth and Planetary Science Letters* **258**, 293–306.

GANSSER A. 1981. The geodynamic history of the Himalaya. *In* Gupta H. K. and Delany F. M. (eds.) *Zagros-Hindukush-Himalaya: Geodynamic Evolution*, pp. 11–21, American Geophysical Union, Washington, DC.

GAO S., LUO T. C., ZHANG B. R. *et al*. 1998a. Chemical composition of the continental crust as revealed by studies in East China. *Geochimica et Cosmochimica Acta* **62**, 1959–75.

GAO S., ZHANG B. R., JIN Z. M., KERN H., LUO T. C. & ZHAO Z. D. 1998b. How mafic is the lower continental crust? *Earth and Planetary Science Letters* **106**, 101–17.

HAN X. M., ZHOU R. Q. & ZHOU Z. H. 1996. Review on the study of volcanic geology in Tengchong, Yunnan Province. *Seismololical and Geomagnetic Observation and Research* **17**, 20–30 (in Chinese with English abstract).

HART S. R. 1984. A large-scale isotope anomaly in the southern Hemisphere mantle. *Nature* **309**, 753–7.

HIRAJIMA T., ZHANG R. Y., LI J. J. & CONG B. L. 1992. Nyboite from the Donghai area, Jiangsu province, eastern China. *Mineral Magazine* **56**, 37–46.

IRVINE T. N. & BARAGAR W. R. A. 1971. A guide to the chemical classification of the common volcanic rocks. *Canadian Journal of Earth Sciences* **8**, 523–8.

JI J. Q. 1998. *Petrology and Cenozoic lithosphere tectonic evolution of Tengchong-Yingjiang-Nabang area, west Yunnan, south-west China*. PhD dissertation, Chinese Academy of Sciences, pp. 1–88 (in Chinese with English summary).

JIANG C. S. 1998. Period division of volcano activities in the Cenozoic era of Tengchong. *Journal of Seismological Research* **21**, 320–9 (in Chinese with English abstract).

JIANG C. S., ZHOU R. Q. & ZHAO C. P. 2003. The relationship between the tectonic geomorphic feature and volcano activity in Tengchong region. *Journal of Seismological Research* **26**, 262–7 (in Chinese with English abstract).

JIANG C. S., ZHOU Z. H. & ZHAO C. P. 2004. The structure characteristics of the crust and upper mantle in the area of Tengchong volcano. *Journal of Seismological Research* **27**, 1–6 (in Chinese with English abstract).

JIN X. C. 2002. Permo-Carboniferous sequences of Gondwana affinity in southwest China and their paleogeographic implications. *Journal of Asian Earth Sciences* **20**, 633–46.

KAN R. J. & ZHAO J. M. 1994. Crust–mantle structure of Tengchong volcanic area. *In* Chen Y. T., Kan R. J., Teng J. W. and Wang C. Y. (eds.) *Advances in Solid Earth Geophysics in China*, pp. 23–30, Oceanic Press, Beijing. (in Chinese).

KATO T., ENAMI A. & ZHAI M. 1997. Ultrahigh-pressure marble and eclogite in the Su-Lu ultrahigh-pressure terrane, eastern China. *Journal of Metamorphic Geology* **15**, 169–82.

LAI S. C., LIU C. Y. & O'REILLY S. Y. 2001. Petrogenesis of the Tertiary high-K calc-alkaline volcanic rocks in north Qiangtang and its geodynamical inplications. *Science in China (Series D)* **31** (Suppl.), 34–42 (in Chinese).

MCDERMOTT F. & HAWKESWORTH C. J. 1991. Th, Pb and Sr isotopic variations in young island arc volcanic and oceanic sediments. *Earth and Planetary Science Letters* **104**, 1–15.

MILLER C., SCHUSTE R., KLOTZLI U., FRANK W. & PURTSCHELLER F. 1999. Post-collisional potassic and ultrapotassic magmatism in SW Tibet: Geochemical and Sr-Nd-Pb-O isotopic constraints for mantle source characteristics and petrogenesis. *Journal of Petrology* **40**, 1399–424.

MO X. X., ZHAO Z. D., DENG J. F. *et al*. 2006. Petrology and geochemistry of postcollisional volcanic rocks from the Tibetan plateau: Implications for lithosphere heterogeneity and collision-induced asthenospheric mantle flow. *In* Dilek Y. and Pavlides S. (eds.) *Postcollisional Tectonics and Magmatism in the Mediterranean Region and Asia*, pp. 507–30, The Geological Society of America, Washington, DC.

MU Z. G., TONG W. & CURTIS G. H. 1987. Timing of Tengchong volcanic activities and related magmatic source. *Acta Geophysica Sinica* **30**, 261–70 (in Chinese with English abstract).

PLATT J. P. & ENGLAND P. C. 1994. Convective lithospheric thinning beneath mountain belts: Thermal and mechanical consequences. *American Journal of Sciences* **294**, 349–53.

POWELL C. M. C. A. & JOHNSON B. D. 1980. Constraints on the Cenozoic position of Sundaland. *Tectonophysics* **63**, 91–109.

QIN J. Z., HUANGFU G., LI Q., QIAN X. D., SU Y. J. & CAI M. J. 2000. 3-D Chromatography of velocity structure in Tengchong volcano areas and nearby. *Journal of Seismological Research* **23**, 850–7 (in Chinese with English abstract).

RAPP R. P., SHIMIZU N. & NORMAN M. D. 2003. Growth of early continental crust by partial melting of eclogite. *Nature* **425**, 605–9.

RICKWOOD P. C. 1989. Boundary lines within petrologic diagrams which use oxides of major and minor elements. *Lithos* **22**, 247–63.

RUPPEL C. 1995. Extensional processes in continental lithosphere. *Journal of Geophysical Research* **100**, 24187–215.

SUN S. S. & MCDONOUGH W. F. 1989. Chemical and isotopic systematics of oceanic basalts: Implications for mantle composition and processes. *In* Saunders A. D. and Norry M. J. (eds.) *Magmatism in the Ocean Basins*, Vol. 42, pp. 313–45, Geological Society Special Publication, Washington, DC.

TAPPONIER P., MERCIER J. L., PROUST F. *et al.* 1981. The Tibetan side of the Indian-Eurasian collision. *Nature* **294**, 405–10.

TAPPONIER P. & MOLNAR P. 1977. Active faulting and tectonics in China. *Journal of Geophysical Research* **82**, 29105–30.

TAPPONIER P., PELTZER G., LE DAIN A. Y., ARMIJO R. & COBBOLD P. 1982. Propagating extrusion tectonics in Asia: New insights from simple experiments with plasticine. *Geology* **10**, 611–6.

TONG W. & ZHANG M. 1989. *Tengchong Geothermics*. Science Press, Beijing (in Chinese).

TURNER S., ARNAUD N., LIU J. *et al.* 1996. Post-collision, shoshonitic volcanism on the Tibetan Plateau: Implications for convective thinning of the lithosphere and the source of the ocean island basalts. *Journal of Petrology* **37**, 45–71.

WANG C. Y. & HUANGFU G. 2004. Crustal structure in Tengchong volcano-geothermal area, west Yunnan, China. *Tectonophysics* **380**, 69–87.

WANG J. H., YIN A., HARRISON T. M., GROVE M., ZHANG Y. Q. & XIE G. H. 2001. A tectonic model for Cenozoic igneous activities in the eastern Indo-Asian collision zone. *Earth and Planetary Science Letters* **188**, 123–33.

WANG Y., ZHANG X. M., JIANG C. S., WEI H. Q. & WAN J. L. 2007. Tectonic controls on the late Miocene-Holocene volcanic field along the southern margin of the Tibetan plateau. *Journal of Asian Earth Sciences* **30**, 375–89.

XIANG C. Y., ZHOU Z. H. & JIANG C. S. 2000. The petrochemistry of the volcanic rocks in Tengchong. *Yunnan Geology* **19**, 134–51.

XIE G. H., LIU C. Q., MASUDA A. & SHIMIZU A. 1992. The geochemical characteristics of Cenozoic volcanic rocks in the area of the Tibetan Plateau. *In* Liu C. Q. (ed.) *Geochronology and Geochemistry of Cenozoic Volcanic Rocks in China*, pp. 400–27, Seismology publishing house, Beijing.

XIE X., YAN M., LI L. & SHEN H. 1989. Usable values for Chinese standard reference samples of stream sediments, soils, and rocks: GSD 9-12, GSS 1-8 and GSR 1-6. *Geostandards. Newsletter* **9**, 277–80.

YANG J., GODARD G., KIENAST J. R., LU Y. & SUN J. 1993. Ultrahighpressure 60 kbar magnesite-bearing garnet peridotites from northeastern Jiangsu. *China Journal of Geology* **101**, 541–54.

Yunnan Bureau of Geology and Mineral Resources 1979. *Tengchong geologic map (1:200000)* (in Chinese).

ZHANG J. J., ZHONG D. L., JI J. Q., DING L. & SANG H. Q. 2001. The structural-chronological frame of the eastern Himalayan syntaxis since the India-Asia collision and its correlation with the Ailaoshan-Red River structural belt. *Bulletin of Mineralogy Petrology and Geochemistry* **20**, 243–4.

ZHANG R. Y., HIRAJIMA T., BANNO S., CONG B. & LIOU J. G. 1995. Petrology of ultrahigh-pressure metamorphic rocks in southern Sulu region, eastern China. *Journal of Metamorphic Geology* **13**, 59–675.

ZHANG R. Y., LIOU J. G. & CONG B. 1994. Petrogenesis of garnet-bearing ultramafic rocks and associated eclogites in the SuLu ultrahigh-P metamorphic terrane, eastern China. *Journal of Metamorphic Geology* **12**, 169–86.

ZHAO C. H. & CHEN T. F. 1992. A discussion on magmatectonic type of Cenozoic volcanism from Tengchong area (Yunnan Province) – A new type of post-collision arc-volcanism. *Geoscience* **6**, 119–29 (in Chinese with English abstract).

ZHAO C. P., RAN H. & CHEN K. H. 2006. Present-day magma chambers in Tengchong volcano area inferred relative geothermal gradient. *Acta Petrologica Sinica* **22**, 1517–28 (in Chinese with English abstract).

ZHAO Z. D., MO X. X., ZHANG S. Q. *et al.* 2001. Post-collisional magmatism in Wuyu Basin, Central Tibet: Proof for the recycle of the Tethys oceanic crusts. *Science in China (Series D)* **31** (Suppl.), 20–6.

ZHOU Z. H., XIANG C. Y. & JIANG C. S. 2000. Geochemistry of the rare earth and trace elements in the volcanic rocks in Tengchong, China. *Journal of Seismological Research* **23**, 215–30 (in Chinese with English abstract).

ZHU B. Q., MAO C. X., LUGMAIR G. W. & MACDOUGALL J. D. 1983. Isotopic and geochemical evidence for the origin of Plio-Pleistocene volcanic rocks near the Indo-Eurasian collisional margin at Tengchong, China. *Earth and Planetary Science Letters* **65**, 263–75.

ZINDLER A. & HART S. R. 1986. Chemical geodynamics. *Annual Review of Earth and Planetary Science letters* **14**, 493–571.